Journal of Molecular Structure 1269 (2022) 133758

Contents lists available at ScienceDirect

Journal of Molecular Structure

journal homepage: www.elsevier.com/locate/molstr

Synthesis of new thiourea derivatives and metal complexes: Thermal behavior, biological evaluation, *in silico* ADMET profiling and molecular docking studies

Tuncay Yeşilkaynak[a,*], Fatma Nur Özkömeç[b], Mustafa Çeşme[c], Ruken Esra Demirdöğen[d], Emine Kutlu[e], Hatice Mehtap Kutlu[f], Fatih Mehmet Emen[e]

[a] *Afsin Vocational School, Kahramanmaraş Sütcü İmam University, 46500, Kahramanmaras, Kahramanmaras TR46500, Turkey*
[b] *Department of Biology, Faculty of Arts and Science, Kahramanmaraş Sütçü İmam University, Kahramanmaraş TR46040, Turkey*
[c] *Department of Chemistry, Faculty of Arts and Science, Kahramanmaraş Sütçü İmam University, Kahramanmaraş TR46040, Turkey*
[d] *Department of Chemistry, Faculty of Arts and Science, Çankırı Karatekin University, Çankırı TR18100, Turkey*
[e] *Department of Chemistry, Faculty of Arts and Science, Burdur Mehmet Akif Ersoy University, Burdur TR15030, Turkey*
[f] *Department of Biology, Faculty of Science, Eskisehir Technical University, Eskişehir TR26555, Turkey*

ARTICLE INFO

Article history:
Received 9 May 2022
Revised 16 July 2022
Accepted 19 July 2022
Available online 20 July 2022

Keywords:
Thiourea
Thermal behavior
Metal complex
Anticancer
Molecular docking
ADMET

ABSTRACT

In this work, N-((5-bromopyridin-2-yl)carbamothioyl)-2-chlorobenzamide (HL^1) and N-((5-bromopyridin-2-yl)carbamothioyl)furan-2-carboxamide (HL^2) and its Cu, Ni and Co metal complexes were prepared. Elemental analysis, FT-IR, UV–vis.,^{1}H NMR, single crystal XRD techniques, magnetic susceptibility and DTA/TG analysis were used for structural characterization. The thermal behaviors of the HL^1, HL^2 and its complexes were investigated. HL^1 and HL^2 ligands were thermally stable up to 119 and 134 °C, respectively. After the structures of the compounds were characterized, anticancer activity studies were performed, and the effects of different groups on the activity were investigated. Cell viability test MTT was made to determine anticancer activities against MCF-7 breast cancer cells. IC_{50} values for MCF-7 cells were in the range of 2.07 µM – 21.25 µM. The $NiL^1{}_2$ complex showed better antitumor activity when at 2.07 µM concentration in 24 h. For their ADMET properties, ligands and metal complexes have been comprehensively studied *in silico*. Notably, when the physicochemical, pharmacological and ADMET properties of ligands HL^1 and HL^2 were evaluated together with drug similarity parameters, good drug-like behavior of the compounds was revealed. In addition, molecular docking studies were performed to assess the binding interactions between ligands and complex compounds and BRAF (V600E -protein kinase). According to the obtained results, it was confirmed that all synthesized compounds exhibited high binding affinity and had an inhibitory effect against BRAF (V600E) protein kinase. The results obtained with both *in vitro* and *in silico* approaches have shown that the synthesized compounds can be evaluated as potent anticancer agents.

1. Introduction

Coordination compounds are of great importance due to their wide usage areas and hence much effort is devoted to developing new coordination compounds. To this end many different ligands are used to endow these compounds chelating properties. The ligands of preference of choice should meet certain criteria such as having physical and chemical stability, high selectivity toward the targeted analyte, eco-friendliness, facile synthesis, and easy extraction.

Thiourea derivatives were investigated for their extractive, catalytic and bioactive properties (i.e., antibacterial, antifungal and antitumor). *N,N*-dialkyl-N'-benzoylthiourea (DABT) derivatives have been used for forming water-insoluble complexes with most of the transition metals as their transition metal complexes are neutral compounds. Especially the ligands bearing donor atoms such as N and O in their structure are very good complexants.

The pioneering studies on thioureas were on synthesis of N-carbamothioylacetamide and since then the number of studies increased until today [1]. *N,N*-dialkyl-*N'*-benzoylthioureas, with their synthesis and application studies, shed light on many important studies in coordination chemistry. Many complex compounds that these derivatives formed with transition metal ions (i.e., Cu (II), Ni (II), Co (II), Pd (II) and Pt (II)) were used in different

* Corresponding author.
E-mail address: tyesilkaynak@ksu.edu.tr (T. Yeşilkaynak).

https://doi.org/10.1016/j.molstruc.2022.133758
0022-2860/

applications [2–7]. Thioureas can form hydrogen bonds with donor atoms (i.e., sulfur and nitrogen) in their structure. Therefore, their behavior differ in different solvents and especially in water [8]. Moreover, thioureas can form hydrogen bonds among themselves via the compounds containing electronegative atoms in their structures. This is of great importance in protonation and deprotonation reactions. Many different thiourea derivatives with different properties can be obtained as result of the interaction of hydrogen atoms in the thiourea compound with different ligand groups.

Thiourea derivatives demonstrate broad-spectrum bioactivity. These studies are not systematic, and their mechanisms could not be elucidated fully yet. Benzoyl thiourea derivatives and their metal complexes were reported for their antibacterial [9–11], antifungal [12–14], antitumor [15–19], antiviral [2], antithyroid [20], antioxidant [19,21–23] properties.

Binding of the proteins to the correct metal is determined by the metal ions or the donor ligands preferred in forming the bioactive agents and this in turn enable the protein to fold and function properly [24]. The relative stabilities of the complexes that the transition metals form are given in Irving–Williams Series.The preferred binding order for the divalent transition metal ions of the fourth period proceeds in the order Mn(II) < Fe(II) < Co(II)< Ni(II) < Cu(II) > Zn(II) [25]. However, there are exceptions when this order is not followed such as when the metal homeostasis is compromised or when the proteins bind less competitive metal ions at the upper end of this Irving–Williams series. In this case, these proteins do not bind to the right metal co-factor. Cu(II) and Co(II) interact with the membrane of the bacteria and induce synthesis of reactive oxygen species (ROS) -by-products of metabolism [26] and cause oxidative stress to bacteria membrane and hence are lethal for bacteria cells. ROS synthesis induced by metal complexes damage cell membranes, proteins, DNA and intracellular system [27]. As a result, highly reactive radicals capable of cell destruction are formed [28]. The electrostatic interactions in the metal ion-bacteria interface arising from the interaction between the metal ion surfaces and the bacteria membrane, which is also called “contact killing”, leads to neutralization of the surface charge of the bacteria membrane which in turn mediates electrostatic interaction among the bacteria membrane and different chemical units [29,30]. The surface charge neutralizes due to the balancing interaction between the positively charged metal ions and the negatively charged phosphate and carboxylate units on the lipid membranes of the bacteria that alters the membrane permeability leading to antimicrobial activity [30,31].

Thermal degradation of thiourea-derived compounds have also been investigated. The thermal decomposition reactions of N-(1,10 -biphenyl)−2-chlorobenzoylthiourea complexes of Co(II), Ni (II) and Cu (II) metal ions were examined and the intermediate products formed were characterized. It was determined that the N-(1,10 -biphenyl)−2-chlorobenzoylthiourea complexes of Ni (II) and Cu (II) complexes degraded in three steps and the Co (II) complex degraded in foursteps [19]. Complexes of 2-Chloro-N-((5-chloropyridine-2-yl)carbamothioyl)benzamide with Co(II), Ni(II) and Cu(II) ions were synthesized and their thermal degradation mechanisms were investigated using thermogravimetric and differential thermal analysis methods. The degradation kinetics of the prepared complexes were investigated via DTA/TG curves. It was determined that the 2-Chloro-N-((5-chloropyridine-2-yl)carbamothioyl)benzamide complexes of Ni (II) and Co (II) ions degraded in threesteps, while the Cu (II) complex degraded in foursteps [22].

In this study new N-((5-bromopyridin-2-yl)carbamothioyl)−2-chlorobenzamide (HL^1: $C_{13}H_9BrClN_3OS$) and N-((5-bromopyridin-2-yl)carbamothioyl)furan-2-carboxamide (HL^2: $C_{11}H_8BrN_3O_2S$)ligands and their transition metal (Co (II), Ni (II) and Cu (II)) complexes were synthesized. The crystal structures of HL^1 and HL^2, their thermal and antitumor properties were investigated and their ADMET was studied. Moreover, molecular docking analysis was performed to investigate the compound-protein interactions and the anticancer potential of the compounds was assessed using *in silico* approaches.

2. Materials and methods

2.1. Materials and instrumentation

All the chemicals used were of reagent quality and were obtained commerciallly from Aldrich or Merck. FT-IR spectra of the compounds were recorded by Perkin Elmer LX-125000B FT-IR instrumentand scanning was made from 400 to 4000 cm^{-1}. The UV–vis. spectra were obtained via a Shimadzu UV-1800 spectrophotometer and scanning was made in the range from 200 to 800 nm. The ^{1}HNMR spectra were obtained on a Bruker Avance III 400 MHz NMR instrument. $CDCl_3$ was used as solvent and TMS was used as the internal standard. The elemental analyses (C, H, N) were performed using a Costech ECS 410 device. In order to complete the combustion process, copper and tungsten oxide were used as catalysts. TG/DTA curves were recorded on a SEIKO-II. Magnetic susceptibilities of the synthesized compounds were determined on Gouy balance model 7550 using $Hg[Co(NCS)_4]$ as standard. The single crystals grown from their ethanol solutions were investigated via X-ray diffraction analysis. The crystallographic data regarding the ligand was obtained via Bruker D8 Venture single-crystal XRD by using PHOTON 100 CMOS detector and KryoFlexII low-temperature device operating at 100 K and MoK_α monochromatized radiation (λ=0.71073 Å).

The multiscan technique was used to correct the data for absorption effects. Direct methods were used for structural characterization and by using SHELXL 2013, the data was refined on F^2 via full-matrix least-squares [32]. Anisotropic displacement parameters were used to refine non-H atoms. Mercury CSD 3.5.1 and Olex2 software were used to prepare the molecular structure plots [33,34]. The crystal and instrumental parameters were exploited and given in the supporting file to determine the unit-cell and data were acquired. For HL^1 and HL^2, the CCDC 2,125,519 and 2,125,607 contain supplementary crystallographic data in this study.

Using Bruker SHELXTL Software Package, the structure was resolved and refined. The molecule with the formula $C_{13}H_9BrClN_3OS$ (HL^1) was found to have space group of $P2_1/c$ and $Z = 4$. The final anisotropic full-matrix least-squares refinement of the observed data on F^2 that had 1.022 variables was found to converge at $R_1 = 6.43\%$ and for all data obtained $wR_2 = 8.65\%$. The goodness-of-fit was 1.022. The final difference in electron density of the synthesized HL^1 exhibited the largest peak of 0.250 $eÅ^{-3}$ and the largest hole of −0.520 $eÅ^{-3}$. According to the final model, the calculated density was 1.686 g/cm^3 and F(000), 736. The molecule with the formula $C_{11}H_8BrN_3O_2S$ (HL^2) was found to have space group of $P2_1/n$ and Z=4. The final anisotropic full-matrix least-squares refinement of the observed data on $F^2$with 648 variables was found to converge at $R_1 = 16.51\%$ and for all the data observed $wR_2 = 15.76\%$. The goodness-of-fit was 0.982. The final difference in electron density of the synthesized HL^2 exhibited the largest peak of 0.320 $eÅ^{-3}$and the largest hole of −0.530 $eÅ^{-3}$. According to the final model, the calculated density was 1.756 g/cm^3 and F(000), 648. The pH measurements were made by using Mettler Toledo MP 220 pH-meterequipped with a combined electrode, and glass electrode was used as the reference electrode. The accuracy of the pH measurements was ±0.05.

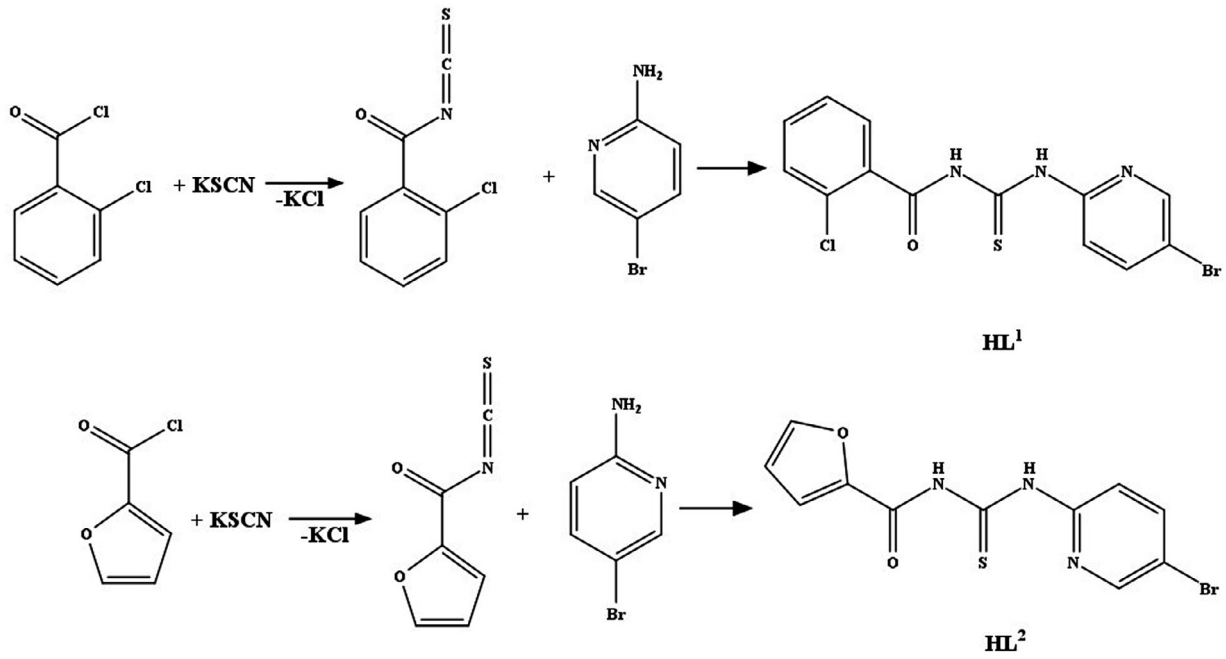

Fig. 1. The reaction scheme for HL^1 (a) and HL^2 (b).

2.2. Synthesis of compounds

2.2.1. Preparation of ligands

All chemicals were used without further purification. 0.01 mol of 2-chlorobenzoyl chloride for HL^1 and furan-2-carbonyl chloride for HL^2 was dissolved in 50 mL acetone. This solution was added dropwise to 0.01 mol of KSCN in 30 mL acetone. The solution was heated under reflux for 40 min and was cooled to RT. Then this mixture was mixed with solution of 2-amino-5–bromo pyridine prepared by dissolving 0.01 mol of it in10 mL acetone under vigorous stirring for 2 h. Then the reaction mixture was poured onto 300 mL of 0.1 mol.L^{-1} HCl. The precipitate was filtered and was washed with deionized water several times. The solid product, which was obtained, was recrystallized from $EtOH/CH_2Cl_2$ [35,36]. The reaction scheme for HL^1 and HL^2 are shown in Fig. 1.

N-((5-bromopyridin-2-yl)carbamothioyl)–2-chlorobenzamide(HL^1): White. Yield: 84%. E. Analysis: C, 41.6; H, 2.6; N, 11.5; S, 8.8; $C_{13}H_9BrClN_3OS$ (cal.: C, 42.1; H, 2.5; N, 11.3; S, 8.7%). FT-IR (ATR, cm^{-1}): υ(Ar-N-H) 3673, υ(N–H) 3162, υ(C–H Ar-H) 2988, υ(C = O) 1677 (s), υ(C = S) 1151, υ(C-Br) 759, υ(C–Cl) 741. ^{1}H NMR (DMSO): 8.75 (m, 1H, NH), 8.65 (m, 2H, Ar-NH), 8.59–7.43 (s,4H, Ar-H), 6.78–6.76 (m, 3H, Ar-H) ppm.

N-((5-bromopyridin-2-yl)carbamothioyl)furan-2-carboxamide (HL^2): Yellow. Yield: 85%. E. Analysis: C, 40.1; H, 3.0; N, 13.0; S, 9.7; $C_{11}H_{10}BrN_3O_2S$ (cal.: C, 40.3; H, 3.1; N, 12.8; S, 9.8%). FT-IR (ATR, cm^{-1}): υ(Ar-N-H) 3681, υ(N–H) 3109, υ(C–H *aro.*) 2970, υ(C = O) 1675 (s), υ(C = S) 1158, υ(C-Br) 758. ^{1}H NMR (DMSO): 8.60 (m, 1H, NH), 8.17–8.15 (m, 2H, Ar-NH), 8.11–7.83 (s, 3H, Ar-H), 6.84–6.56 (m, 3H, Ar-H) ppm.

2.2.2. Preparation of metal complexes

Co(II), Ni (II) and Cu (II)complexes of HL^1 and HL^2 were prepared using reagent grade chemicals according to the general procedure given elsewhere [35,36]. 0.001 mol of $CoCl_2/NiCl_2/CuCl_2$ salts were dissolved in 10 mL of ethanol. HL solution was prepared by dissolving HL (0.002 mol) in 40 mL of Et-OH with a few drops of Et_3N. Metal solutions were added to the ligand solution under vigorous stirring for 30 min. Thus, obtained complexes were filtered, washed with ethanol, and dried. The molecular structures of $M(L^1)_2$ and $M(L^2)_2$ complexes are shown in Fig. 2.

$[Co(L^1)_2]$: Pale green. Yield: 80%. E. Analysis: C, 38.9; H, 2.1; N, 10.8; S, 8.2; $C_{26}H_{16}Br_2Cl_2N_6O_2S_2Co$ (cal.: C, 39.1; H, 2.0; N, 10.5; S, 8.0%). FT-IR (ATR, cm^{-1}): υ(Ar-N-H) 3675, υ(C–H Ar-H) 2987, υ(C = N) 1519, υ(C-Br) 745, υ(C–Cl) 698. ^{1}H NMR (DMSO): 8.11–8.09 (m, 4H, Ar-NH), 7.85–7.65 (m, 8H, Ar-H), 7.61–7.40 (m, 6H, Ar-H) ppm.Electronic spectrum, λ_{max} (cm^{-1}): 42,918, 27,933.

$[Ni(L^1)_2]$: Pale green. Yield: 84%. E. Analysis: C, 38.3; H, 2.2; N, 10.7; S, 8.2; $C_{26}H_{16}Br_2Cl_2N_6O_2S_2Ni$ (cal.: C, 39.1; H, 2.0; N, 10.5; S, 8.0%). IR (ATR, cm^{-1}): υ(Ar-N-H) 3674, υ(C–H Ar-H) 2987, υ(C = N) 1531, υ(C-Br) 742, υ(C–Cl) 704. ^{1}H NMR (DMSO): 8.60–8.28 (m, 4H, Ar-NH), 7.93–7.69 (m, 8H, Ar-H), 7.64–7.36 (m, 6H, Ar-H) ppm. Electronic spectrum, λ_{max} (cm^{-1}): 40,946, 32,362.

$[Cu(L^1)_2]$: Pale green. Yield: 83%.E.Analysis: C, 37.9; H, 2.1; N, 10.5; S, 8.2; $C_{26}H_{16}Br_2Cl_2N_6O_2S_2Cu$ (cal.: C, 38.9; H, 2.0; N, 10.5; S, 8.0%). IR (ATR, cm^{-1}): υ(Ar-N-H) 3672, υ(C–H Ar-H) 2964, υ(C = N) 1519, υ(C-Br) 738, υ(C–Cl) 708.Electronic spectrum, λ_{max} (cm^{-1}): 43,872, 32,573.

$[Co(L^2)_2]$: Green. Yield: 79%. E. Analysis: C, 37.2; H, 2.7; N, 11.6, S, 8.7; $C_{22}H_{18}Br_2N_6O_4S_2Co$ (cal.: C, 37.1; H, 2.5; N, 11.8; S, 9.0%). IR (ATR, cm^{-1}): υ(Ar-N-H) 3674, υ(C–H *aro.*) 2901, υ(C=N) 1519, υ(C-Br) 757. ^{1}H NMR (DMSO): 8.98–8.48 (m, 4H, Ar-NH), 8.37–8.02 (m, 6H, Ar-H), 7.96–7.10 (m, 6H, Ar-H) ppm. Electronic spectrum, λ_{max} (cm^{-1}): 39,702, 30,864.

$[Ni(L^2)_2]$: Pale green. Yield: 81%. E. Analysis: C, 36.8; H, 2.7; N, 11.8, S, 8.7; $C_{22}H_{18}Br_2N_6O_4S_2Ni$ (cal.: C, 37.1; H, 2.5; N, 11.8; S, 9.0%). IR (ATR, cm^{-1}): υ(Ar-N-H) 3666, υ(C–H *aro.*) 2885, υ(C=N) 1580, υ(C-Br) 742. ^{1}H NMR (DMSO): 9.01–8.63 (m, 4H, Ar-NH), 8.56–8.01 (d, 6H, Ar-H), 7.90–7.10 (m, 6H, Ar-H) ppm. Electronic spectrum, λ_{max} (cm^{-1}): 40,480, 32,468.

$[Cu(L^2)_2]$: Green. Yield: 78%. E. Analysis: C, 37.1; H, 2.6; N, 11.5, S, 8.6; $C_{22}H_{18}Br_2N_6O_4S_2Cu$ (cal.: C, 36.8; H, 2.5; N, 11.7; S, 8.9%). IR (ATR, cm^{-1}): υ(Ar-N-H) 3672, υ(C–H *aro.*) 2900, υ(C=N) 1592, υ(C-Br) 743. Electronic spectrum, λ_{max} (cm^{-1}): 40,262, 29,940.

2.3. Determination of anticancer activity

The method reported by Junkyu Han et al. was used in anticancer activity studies [37]. Standard MTT bioassay was used for *in vitro* cytotoxicity study of thesynthesized compounds on cancer cell lines at 24 h drug exposure. Human breast cancer

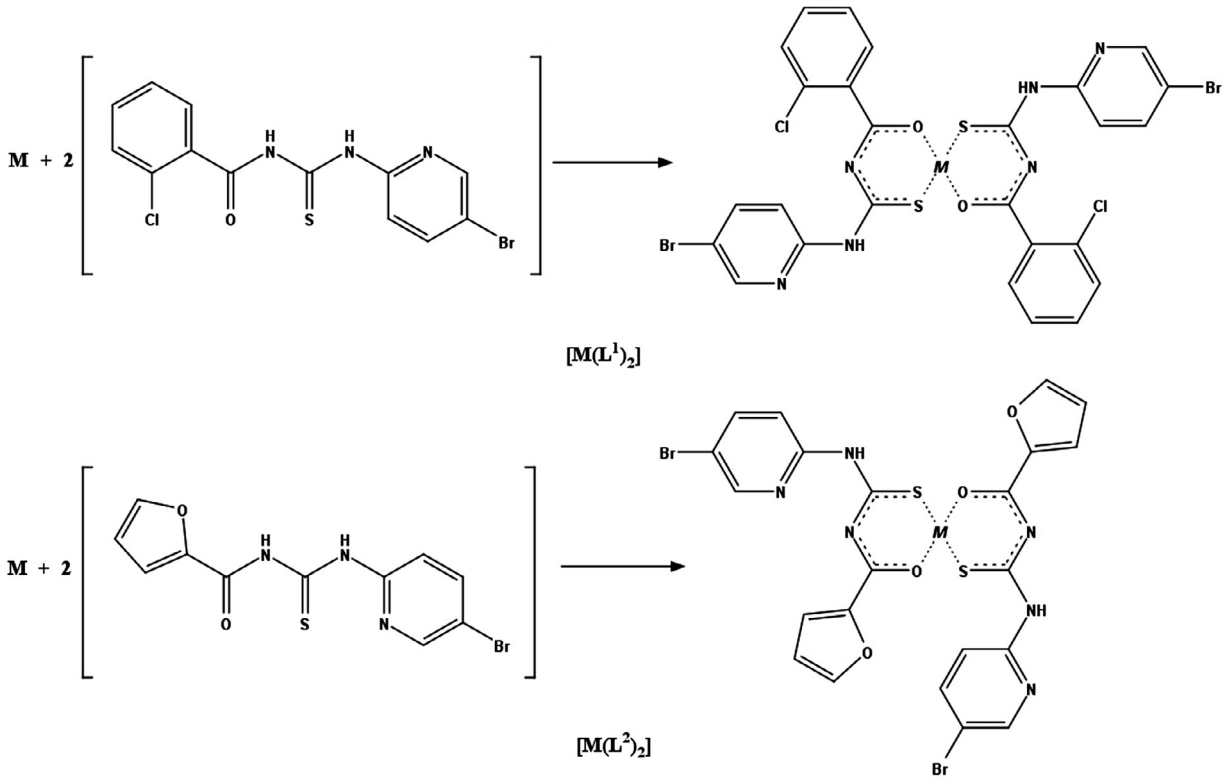

Fig. 2. The reaction scheme for $M(L^1)_2$ (a) and $M(L^2)_2$ (b). (M= Co, Ni, Cu).

cells (MCF-7) were used to determine the compounds with high bioactivity and assess the efficiency of the compounds. The MCF-7 cells were purchased from ATCC and were cultured in RPMI-1640 mediumcontaining 10% FBS, 1% 5.000 U/mL of penicillin and 5.000 U/mL streptomycinunder 5% CO_2 atmosphere at 37 °C incubator conditions. The incubated MCF-7 cells (5×10^3 cells/per well) were seeded on 96 well platesseparately for to test each complex in triplicates and then they were further incubated for 24 h under the same incubator conditions. Then, the supernatant of all the wells that contain attached MCF-7 cells were exchanged with solutions of the test complexes (prepared in RPMI-1640 medium) at concentrations of 3.125, 6.25, 12.50, 25.00, 50 and 100 µM that were placed in separate wells in triplicates according to the labellings of plates. All test plates containing the complexes atwith the mentioned concentrations were incubated for 24 h and 48 h. Then, 20 μL MTT solution (5 mg/mL in PBS) was added to each well and plates were incubated for another 4 h. At the end of incubation, the media were carefully removed, and the MTT formazan was dissolved by adding 200 µL of DMSO (dimethylsulfoxide) to each well. The absorbance measurements were performed via a microplate reader for each well at 540 nm. The growth or viability percentages of the treated and untreated cells was calculated using the formula below. The half maximal inhibitory concentrations (IC_{50}) were detected from the calculated viability percentages and used for further experimentations.

$$Growthrate = \left(\frac{absorbancetreatedwells}{absorbanceuntreatedwells}\right) \times 100$$

2.4. In silico *ADMET studies*

SwissADME web tools (www.swissadme.ch) were used to evaluate the physicochemical and pharmacological properties of the compounds and display them against Lipinski RO5. Smile notations of synthetic compounds and chemical structures were obtained with ChemDraw 20.0 software. The smile notations of the compounds were then fed into swissADME to calculate many molecular ADME properties [38]. A web-based platform, pkCSM, was used to predict the toxicological outcomes of compounds [39].

2.5. Molecular docking studies

In this study, 3D structures of the compounds were obtained via ChemDraw 20.0 software. The 3D structures of all the compounds were energy minimized using the MM2 minimization algorithm via Chem3D 20. The molecular docking studies were performed using PyRx (Autodock Vina) docking (academic licensed version 0.9.9) software to determine the binding energy and interactions of the synthetic compounds with the target protein BRAF (PDB ID: 4R5Y). During this analysis, flexible-ligand:rigid-receptor docking conditions were chosen [40,41]. The grid on the ligand-binding pocket of the protein 4R5Y was positioned at the binding site of X:16.93, Y:10.68, Z:−14.56, and the grid size were $29 \times 41 \times 38$ $Å^3$ dimensions with 0.375 Å. Discovery Studio 2021 was used to show and analyze the findings of the optimum docking positions for the interaction and the binding affinities. The resulting binding energies (kcal/mol)) give a score based on the best-docked protein-ligand complex selected.

3. Results and discussion

3.1. FT-IR

The FT-IR vibration bands of the HL^1 and HL^2 ligands and their metal (Co, Ni and Cu) complexes are given in Tables 1 and 2. The bands observed at 3673 $cm^{-1}$for HL^1 and 3681 cm^{-1} for HL^2 in the

Table 1
FT-IR frequency data of HL^1 and its metal complexes (cm^{-1}).

Comp.	Aro-(N–H)	(N–H)	(C–H)	(C=O)	(C=N)	(C=S)	(C-Br, C–Cl)
HL^1	3673	3162	2988	1677	–	1151	759–741
$Co(L^1)_2$	3675	–	2987	–	1519	–	745–698
$Ni(L^1)_2$	3674	–	2987	–	1531	–	742–704
$Cu(L^1)_2$	3672	–	2964	–	1519	–	738–708

Table 2
FT-IR frequency data of HL^2 and its metal complexes (cm^{-1}).

Comp.	Aro-(N–H)	(N–H)	(C–H)	(C=O)	(C=N)	(C=S)	(C-Br)
HL^2	3681	3109	3139–2970	1675	–	1158–1140	758
$Co(L^2)_2$	3674	–	2987–2901	–	1519	–	757
$Ni(L^2)_2$	3666	–	2987–2885	–	1580	–	742
$Cu(L^2)_2$	3672	–	3187–2900	–	1592	–	743

FT-IR spectrums shows the N–H stretching vibration of the NH_2 group located from the ortho position of the pyridine ring. The stretching vibration bands of the N–H groups outside the ring in the structure is observed as a sharp peak at 3162 cm^{-1} for HL^1 and 3381 cm^{-1} for HL^2. The vibration bands observed at 2988 cm^{-1} for HL^1 and 2970 cm^{-1} for HL^2 indicate the aromatic C–H stretching vibrations, and the bands observed at 1587–1520 cm^{-1} for HL^1 and 1578–1561 cm^{-1} shows the C–C stretching vibrations of the ring. The intense bands observed at 1434–1002 cm^{-1} for HL^1 and 1449–1011 cm^{-1} for HL^2 belong to in-plane C–H bending vibrations. The bands observed at 759 and 741 cm^{-1} for HL^1 belong to C-Br and C–Cl stretching vibrations. The bands observed at 758 cm^{-1} for HL^2 belong to C-Br stretching vibration. The intense bands observed at 1677 cm^{-1} for HL^1 and 1675 cm^{-1} for HL^2 belong to the carbonyl group's stretching vibrations (C=O), and the bands observed at 1151 cm^{-1} for HL^1 and 1158 cm^{-1} for HL^2 belong to the (C=S) stretching vibration. The FT-IR spectrums of ligands are given in supplementary data (Figs. S1 and S2). In the FT-IR spectrums of HL^1's and HL^2's metal complexes, the C=S groups overlap with other bands due to the shift of the vibrational band, and it is difficult to determine in this region. As a result of the complexation reactions, it is observed that the stretching vibrational bands of the carbonyl group (C=O) shift to lower vibrational bands. The stretching vibration band of the N–H group (3162 for HL^1 and 3109 cm^{-1} for HL^2) in the structures remains aprotic due to binding to the metal atom of HL^1 and HL^2, and thus this band cannot be observed in the FT-IR spectra of metal complexes. The N–H bands that cannot be observed in the FT-IR spectra of HL^1 and HL^2 and the shift of C=O and C=S bands indicate that the complexation reaction took place [4,6,19,21,35,42,43].

3.2. ^1H NMR

^1H NMR spectra confirm the proposed structure for HL^1, HL^2, $[CoL^1{}_2]$, $[NiL^1{}_2]$, $[CoL^2{}_2]$ and $[NiL^2{}_2]$. Two peaks observed for HL^1 in the ^1H NMR spectrum at 8.75 ppm (ali.) and 8.65 ppm (aro.), which indicate N–H group. The C–H bonds of the aromatic ring were observed to appear as multiplet peaks at around 8.59–7.43 ppm for ligand. The aliphatic N–H peak is not seen in the complexes. These data provedthat the complexes were formed and confirmed the structure of the proposed complexes. The Ar-(C–H) protons are observed at 7.93–7.36 ppm for the $[NiL^1{}_2]$ and 7.85-7.40 ppm for the $[CoL^1{}_2]$ complex. The aromatic N–H peaks are observed at 8.60–8.28 ppm for $[NiL^1{}_2]$ and 8.11–8.09 ppm for $[CoL^1{}_2]$.

Single and triplet peaks are observed for HL^2 in the ^1H NMR spectrum at 8.60 ppm (ali.) and 8.17–8.15 ppm (aro.) which indicate the N–H group. The C–H bonds of the aromatic ring were observed to appear as multiplet peaks at around 8.11–7.83 ppm for the ligand. The aliphatic N–H peak is not seen in the complexes. These data prove complex formation and confirm the proposed complex structure. The Ar-(C–H) protons are observed at 7.90–7.10 ppm for $[NiL^2{}_2]$ and 7.96- 7.10 ppm for $[CoL^2{}_2]$. The aromatic N–H peaks are observed at 9.01–8.63 ppm for $[NiL^2{}_2]$ and 8.98–8.48 ppm for $[CoL^2{}_2]$. Since $[CuL^1{}_2]$ and $[CuL^2{}_2]$ are paramagnetic, their ^1H NMR spectra could not be obtained [19]. The ^1H NMR spectrums of HL^1 and HL^2 are given in the supplementary data (Figs. S3 and S4).

3.3. Magnetic susceptibility of complexes

The magnetic susceptibilities of complex samples of $[CoL^1{}_2]$, $[NiL^1{}_2]$, $[CuL^1{}_2]$, $[CoL^2{}_2]$, $[NiL^2{}_2]$ and $[CuL^2{}_2]$ were investigated at 295 K. Magnetic susceptibilities of the compounds were determined via Gouy balance model 7550 using $Hg[Co(NCS)_4]$ as standard. Magnetic moments were calculated from below formula,

$$\mu = 2.83(\chi MT)^{1/2}$$

where: μ_{eff} - effective magnetic momentum, χ_M - magnetic susceptibility per molecule and T - absolute temperature. The measured values were 4.54 BM; 3.32 BM; 1.84 BM; 4.60 BM; 3.38 BM and 1.88 BM for $[CoL^1{}_2]$, $[NiL^1{}_2]$, $[CuL^1{}_2]$, $[CoL^2{}_2]$, $[NiL^2{}_2]$ and $[CuL^2{}_2]$, respectively. The observed magnetic momentum value of the Co(II) complexes are 4.54 BM and 4.60 BM. These are the expected values that lie from 4.20 to 4.88 BM for the tetrahedral Co(II) complexes, which is the sum of contributions only due to spin moments and spin–orbit couplings. Thus, the Co(II) complex shows the tetrahedral geometry [44,45]. The magnetic momentum value of 3.32 and 3.38 BM for the Ni(II) complexes are in the range of 3.2–4.0 BM expected for the tetrahedral Ni(II) complexes corresponding to two unpaired electrons [45–47]. Cu(II) complexes have μ_{eff} values of 1.84 BM and 1.88 BM which indicate to the presence of one unpaired electron. The magnetic momentum values confirmed the distorted square-planar configuration. Cu(II) square-planar complexes exhibit magnetic momentum in the range 1.8–2.1 BM [44,45,48].

3.4. Crystallographic structure of the ligands

Molecular structure of the HL^1 and HL^2 with the atom numbering schemes are given in Figs. 3 and 5. Crystal data and structure refinement parameters are given in Tables 3 and 4. Some experimental geometric parameters are given in the supporting information (Tables S1–S14). The HL^1 and HL^2 samples with 0.150 mm x 0.100 mm x 0.100 mm approximate dimensions were used for the x-ray crystallographic analysis. The x-ray intensities were measured on a Bruker D8 VENTURE system

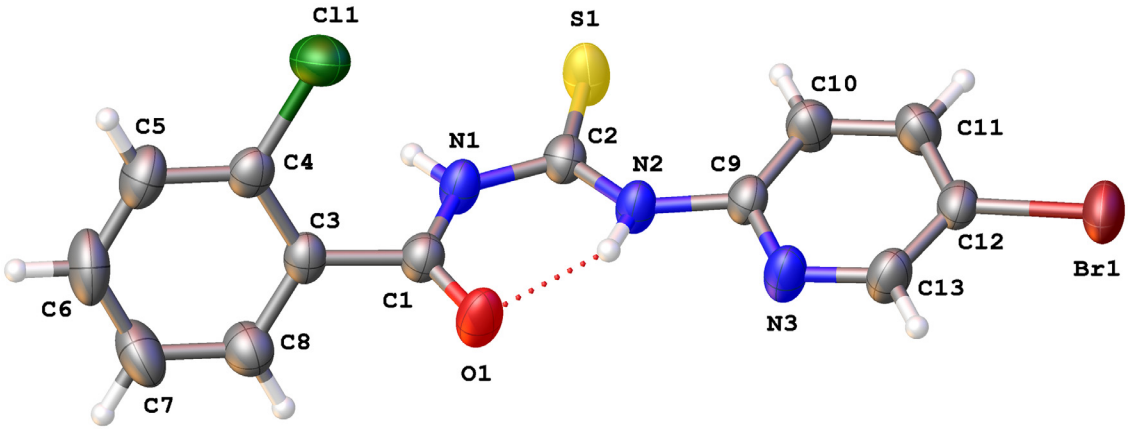

Fig. 3. ORTEP view of the HL^1; thermal ellipsoids are shown at the 50% probability level.

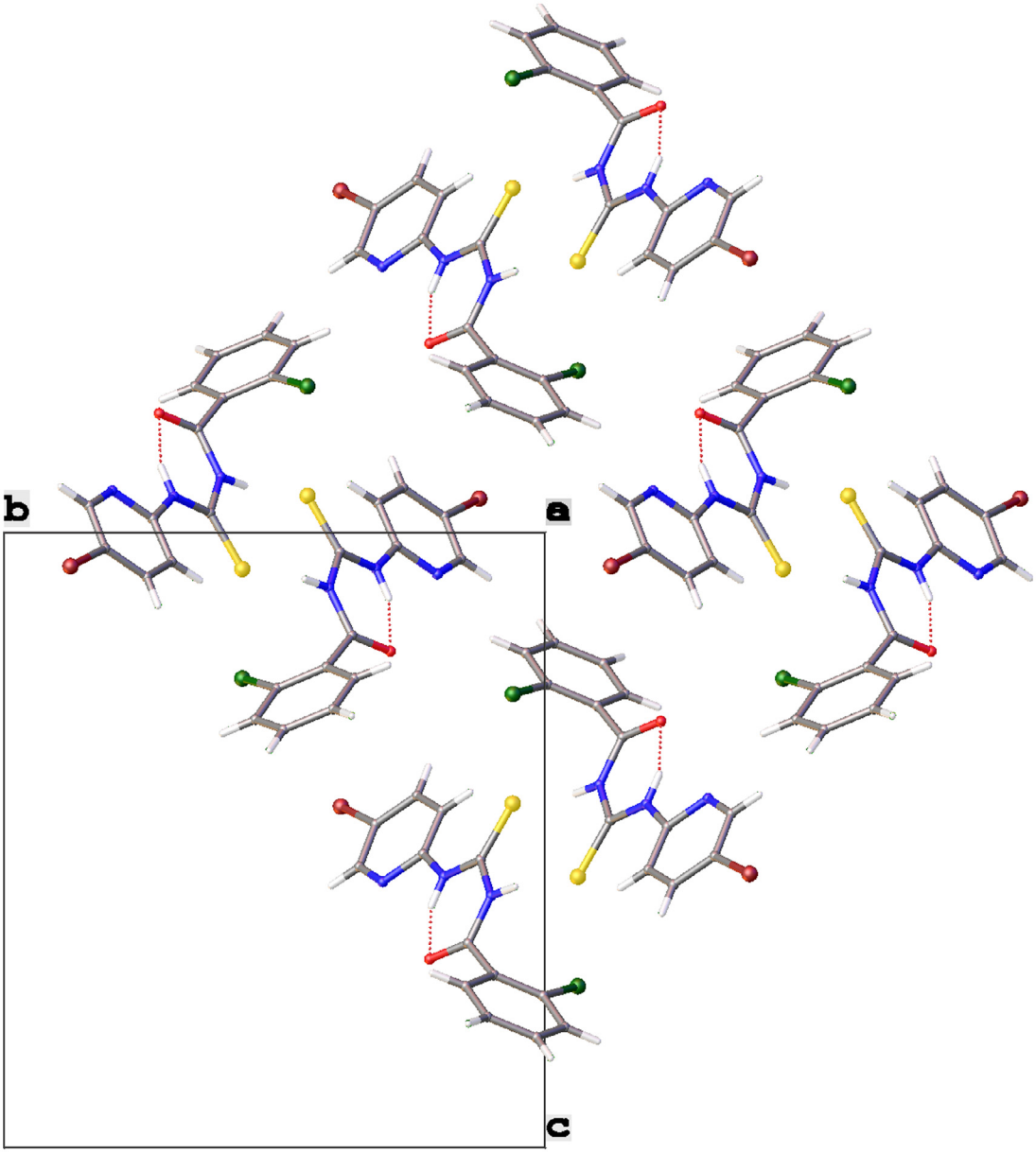

Fig. 4. Crystal packing of the HL^1 in monoclinic system with $P2_1/c$ space group.

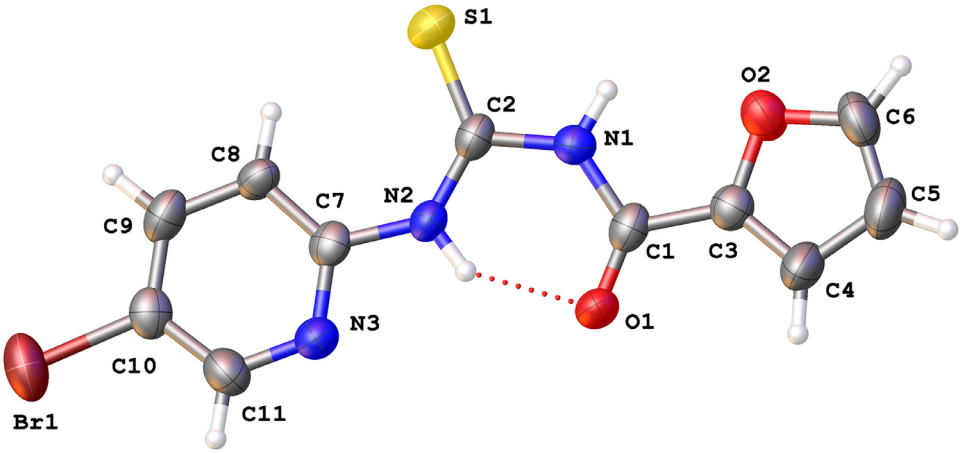

Fig. 5. ORTEP view of the HL^2; thermal ellipsoids are shown at the 50% probability level.

Table 3
Crystal data and structural refinement parameters for the HL^1.

Empirical formula	$C_{13}H_9BrClN_3OS$
Formula weight	370.65
Temperature/K	297.11
Crystal system	monoclinic
Space group	$P2_1/c$
a/Å	6.694(2)
b/Å	13.846(5)
c/Å	15.763(6)
α/°	90
β/°	91.616(14)
γ/°	90
Volume/Å^3	1460.3(9)
Z	4
ρ_{calc}g/cm^3	1.686
μ/mm^{-1}	3.138
F(000)	736.0
Crystal size/mm^3	0.1 × 0.1 × 0.1
Radiation	MoKα (λ = 0.71073)
2Θ range for data collection/°	5.884 to 56.696
Index ranges	−8 ≤h ≤ 8, -18≤ k ≤ 18, -2≤ l ≤ 21
Reflections collected	27,678
Independent reflections	3622 [R_{int} = 0.0580, R_{sigma} = 0.0351]
Data/restraints/parameters	3622/0/181
Goodness-of-fit on F^2	1.022
Final R indexes [I>=2σ (I)]	R_1 = 0.0349, wR_2 = 0.0751
Final R indexes [all data]	R_1 = 0.0643, wR_2 = 0.0865
Largest diff. peak/hole / e Å^{-3}	0.25/−0.52

Table 4
Crystal data and structural refinement parameters for the HL^2.

Empirical formula	$C_{11}H_8BrN_3O_2S$
Formula weight	326.17
Temperature/K	100
Crystal system	monoclinic
Space group	$P2_1/n$
a/Å	11.351
b/Å	8.114
c/Å	13.812
α/°	90
β/°	104.08
γ/°	90
Volume/Å^3	1233.8
Z	4
ρ_{calc}g/cm^3	1.756
μ/mm^{-1}	3.497
F(000)	648.0
Crystal size/mm^3	0.1 × 0.1 × 0.05
Radiation	MoKα (λ = 0.71073)
2Θ range for data collection/°	5.87 to 56.676
Index ranges	−1≤ h ≤ 15, -10 ≤ k ≤ 10, -17 ≤ l ≤ 18
Reflections collected	29,674
Independent reflections	3081 [R_{int} = 0.1786, R_{sigma} = 0.1112]
Data/restraints/parameters	3081/0/163
Goodness-of-fit on F^2	0.982
Final R indexes [I>=2σ (I)]	R_1 = 0.0569, wR_2 = 0.1197
Final R indexes [all data]	R_1 = 0.1651, wR_2 = 0.1576
Largest diff. peak/hole / e Å^{-3}	0.32/−0.53

equipped with a multilayer monochromator and a MoK$_\alpha$ Sealed tube (λ = 0.71073 Å). The frames were integrated with the Bruker SAINT software package using a wide-frame algorithm. The structures were resolved and refined using the Bruker SHELXTL Software Package, using the space groups $P2_1/c$, with Z = 4 for the formula unit, $C_{13}H_9BrClN_3OS$ and $P2_1/n$, with Z = 4 for the formula unit, $C_{11}H_8BrN_3O_2S$.

The proposed crystal structure of the HL^1 is presented in Fig. 3 and in Table 3 is presented the crystal parameters.

The crystal packing is given in Fig. 4. The intramolecular hydrogen interaction can be observed for (N–H… O) [49]. Here the bond length of H–O is 1.907 Å. According to the results obtained in the structural analysis, C2-S1 and C1-O1 bond lengths are found to be 1.657(2) and 1.221(3) Å, respectively. These results suggest a double bond as they lie in the typical average double bond length. The bond lengths of the N1-C2, 1.400(3); N2-C2, 1.338(3) and N1-C1, 1.371(3) Å are indicative of partial double bond. Bond angles of C = O and C = S groups are as follows N1-C2-S1, 118.56(17); N2-C2-S1, 128.07(18); N1-C1-O1, 123.50° (2) and O1-C1-C3, 121.30°(2).

The proposed crystal structure of the HL^2 is presented in Fig. 5 and in Table 4 is presented the crystal parameters. An intramolecular hydrogen interaction can be observed (N–H… O). The bond length of H–O is 1908 Å [49]. The necessary parameters are given as supporting file.

The crystal packing is given in Fig. 6. According to the results obtained in the structural analysis, the bond lengths of C2-S1 and C1-O1 are 1.659(5) and 1.211(6) Å, respectively. These results suggest a double bond as they lie in the typical average double bond length. The bond lengths of N1-C1, 1.390(6); N1-C2, 1.406(5) and N2-C2, 1.334(6) Å are indicative of partial double bond. Bond angles of C = O and C = S groups are N2-C2-S1, 129.30° (3); N1-C2-S1,116.70° (4); N1-C1-O1, 124.40° (4) and O1-C1-C3, 122.50° (4).

3.5. Thermal characacterization of the compounds

DTA-TG analyses of compounds that used 8.00–10.00 mg range sample mass were made at a heating rate of 10 °C/min under N_2 atmosphere. The results for the DTA-TG study of HL^1 is given in

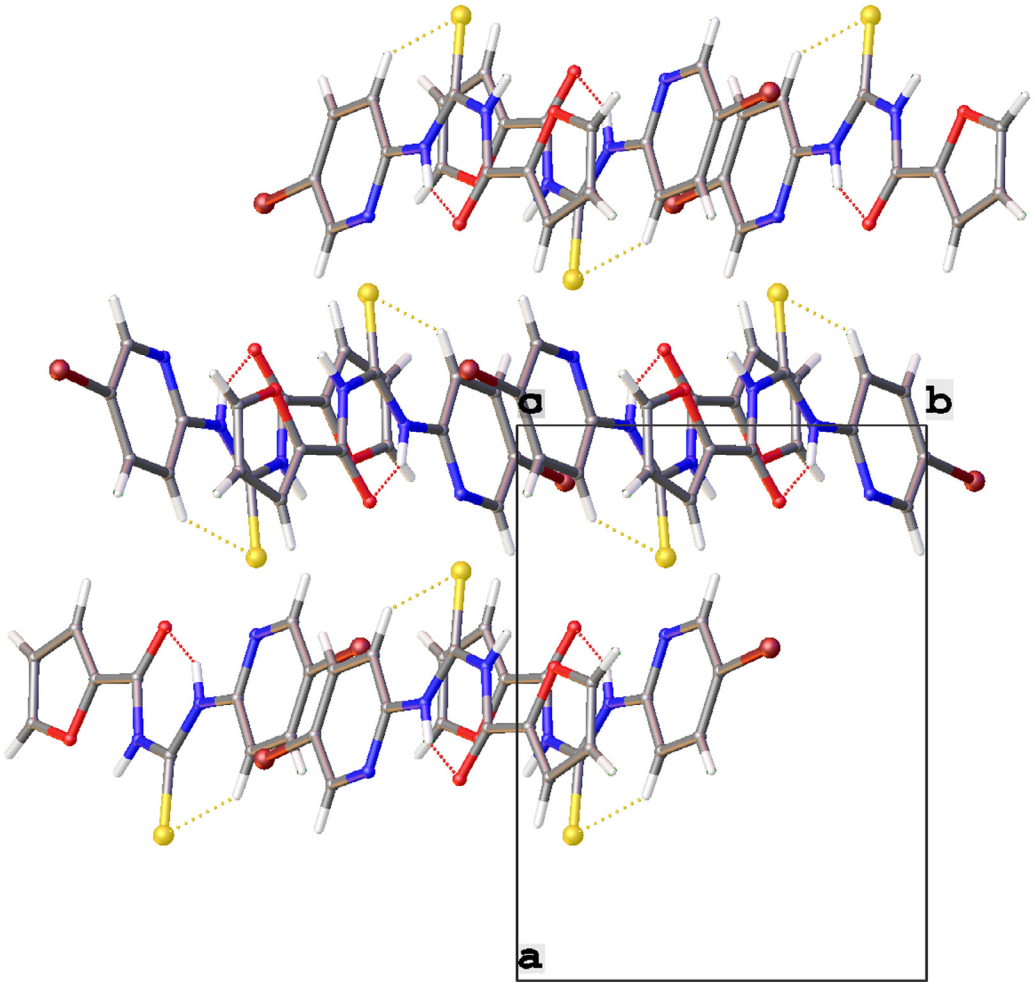

Fig. 6. Crystal packing of the HL^2 in orthorhombic system with $P2_1/n$ space group.

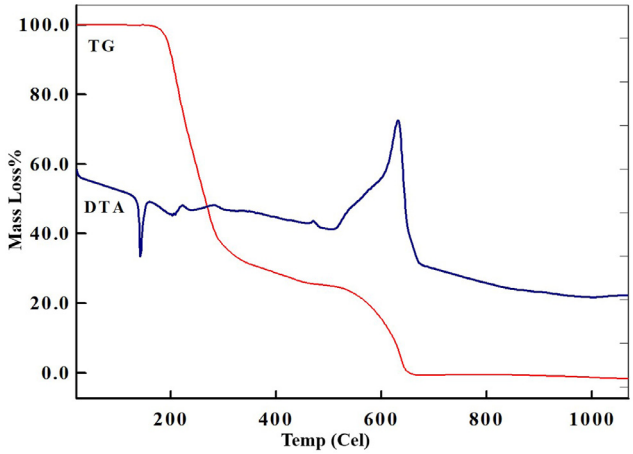

Fig. 7. The DTA-TG diagrams of HL^1.

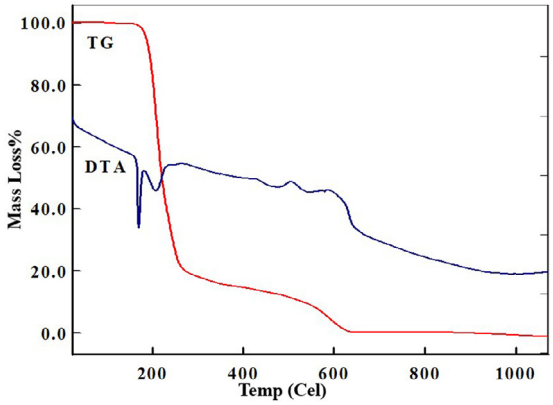

Fig. 8. The DTA-TG diagrams of HL^2.

Fig. 7. The degradation process of HL^1 proceeds over three steps. The first degradation step takes place in the range from 119 °C to 264 °C. 0.5 mol of the ligand was found to leave the structure and the experimental mass loss is 50.00% (calc.:50.00%). The intermediate structure that forms in this step is proposed to be $L_{0.5}$. The second degradation step was shown from 264 °C to 462 °C with mass loss of 24.50% (calc.:25.00%). In this step, 0.25 mol of the ligand were found to leave the structure and were converted into gaseous products. The intermediate structure that forms in this step is proposed to be $L_{0.25}$. In the third degradation step, observed above 462 °C, the experimental mass loss was 25.70%, while the theoretical loss was calculated to be 25.00%. This indicates that 0.25 mol of the ligand have degraded. The thermal degradation studies of the metal complex have been reported in Table 5. In the second degradation stage of the $CuL^1{}_2$ compound, sublimation of the 0.33 mol of the metal is also observed together with the thermal degradation of the ligand [6,50,51].

The result for the DTA-TG study of HL^2 is given in Fig. 8. The HL^2 degrades in three steps. The first degradation step was observed in the range of 134 °C-232 °C. In this step, one 0.6 mol

Table 5
The thermal degradation results of HL^1's metal complexes, $[ML^1{}_2]$.

Comp.	Stage	TG temp. range/°C	Mass loss%		Interm. product (or residue)
			Exper.	Theor.	
$CoL^1{}_2$	I	120–305	29.80	30.96	$CoL_{4/3}$
	II	305–505	14.80	15.48	CoL
	III	>505	47.40	46.43	Co
$NiL^1{}_2$	I	116–318	62.20	61.93	$NiL_{2/3}$
	II	>318	31.20	30.97	Ni
$CuL^1{}_2$	I	127–339	46.50	46.17	CuL
	II	>339	49.50	46.17	Cu

Table 6
The thermal degradation results of HL^2's metal complexes, $[ML^2{}_2]$.

Comp.	Stage	TG temp. range/°C	Mass loss%		Interm. product (or residue)
			Exper.	Theor.	
$CoL^2{}_2$	I	142–243	23.50	23.00	$CoL_{3/2}$
	II	243–311	24.70	23.00	CoL
	III	>311	44.80	46.0	Co
$NiL^2{}_2$	I	143–287	31.10	30.67	$NiL_{4/3}$
	II	287–458	13.40	15.33	NiL
	III	>458	44.80	46.00	Ni
$CuL^2{}_2$	I	151–454	44.10	45.69	CuL
	II	>454	55.00	45.69	–

of the ligand was found to leave the structure, corresponding to an experimental mass loss of 60.00%. The chemical formula for the intermediate formed at the end of this step is proposed to be $L_{0.4}$. The second degradation step took place in the range of 232 °C-268 °C, with an experimental mass loss of 19.10%, while the theoretical mass loss was 20.00%. In this step, 0.2 mol of the ligand was found to leave the structure and turn into gaseous products. The intermediate, which forms, can be represented with the formula $L_{0.2}$. The third decomposition stage was observed at a temperature above 268 °C. After the third degradation step, the ligand is completely degraded. In Table 6 are given the TG results for metal complexes. In the second degradation stage of the $CuL^2{}_2$ compound, sublimation of the metal is also observed together with the thermal degradation of the ligand [6,51,52]. The TG diagrams of complexes are given in supplementary data (Figs. S5 and S6).

3.6. Anticancer activities

The MTT assay was used to investigate the cytotoxic effect of the complexes against MCF-7 breast cancer cells via the method proposed by Han at al [37]. Cell viability was determined via spectrophotometric method and the IC_{50} values for each complex on MCF-7 cells were determined. The viability percentages of MCF-7 cells upon 24 h and 48 h of exposure to the ligands and their metal complexes are presented in Tables 7, 8, 9 and 10. The IC_{50} values of the complexes tested were found to be between 2.07 µM and 21.25 µM. The $NiL^1{}_2$ complex shown best antitumor activity at 24 h with 2.07 µM. Moreover, the IC_{50} values for the HL^1 (2.44 µM, 24 h), $NiL^2{}_2$ (3.99 µM, 24 h), $CuL^1{}_2$ (2.17 µM, 48 h), $CoL^1{}_2$ (2.35 µM, 48 h) and $CuL^2{}_2$ (3.97 µM, 48 h) compounds indicated that they have good antitumor activities.

According to the Irving–Williams Series, the stability of complexing for divalent transition metal ions proceed in the order Mn(II) < Fe(II) < Co(II)< Ni(II) < Cu(II) > Zn(II) [25]. However, there are cases that do not follow this order. For instance, when the metal homeostasis is compromised or when the proteins bind less competitive metal ions at the upper end of this Irving–Williams series is not followed. In this case, these proteins do not bind to the right metal co-factor. The MTT results showed that as compared to the $[ML^2{}_2]$ complexes, the $[ML^1{}_2]$ complexes are more effective against MCF-7 cells. It is seen that Cu(II), Ni(II) and Co(II) are more effective. According to the Irving–Williams series the activities of the complexes are expected to be in the order Co(II)< Ni(II)< Cu(II). However, according the Bohr magneton results, while the synthesized Ni (II) and Co (II) complexes have tetrahedral feometry the Cu(II) complexes have distorted planar square geometry. It is known that different interactions are observed with different geometries. Moreover, cytotoxicity of the complexes cannot be explained only via the type of metal ions and geometry. The structure of the ligands play an important role in protein-ligand interaction. While the HL^1 ligand has 2-chlorophenyl ring in its structure, the HL^2 ligand contains a furan ring. The Cl substituent in the phenyl ring enabled the HL^1 ligand be cytotoxic against the MCF-7 cells at lower concentrations. The results showed that the activity values of $NiL^1{}_2$ (24 h) and $CuL^1{}_2$ (48 h) compounds were observed to be very close to each other.

Table 7
The viability percentages at 24 h of HL^1 and it's complexes on MCF-7 cells.

24h	HL^1		$NiL^1{}_2$		$CuL^1{}_2$		$CoL^1{}_2$	
Doses (µM)	Viability (%)	Standard Deviation(±)	Viability (%)	Standard Deviation(±)	Viability (%)	Standard Deviation(±)	Viability (%)	Standard Deviation(±)
100	11.75	3.96	14.62	7.78	5.29	2.04	1.76	0.10
50	25.93	9.23	15.41	2.22	8.05	0.51	3.87	1.89
25	23.69	0.26	18.08	2.00	8.65	4.42	5.99	0.50
12.5	34.70	7.92	24.37	1.56	21.15	15.98	6.55	1.49
6.25	28.36	12.66	25.00	1.11	36.18	17.85	8.59	0.40
3.125	36.01	9.76	24.37	4.22	81.37	2.89	83.87	8.66
Control	99.81	2.37	100.16	0.67	100.12	6.63	100.07	13.25
IC_{50} (µM)	2.44		2.07		8.35		9.66	

Table 8
The viability percentages at 24 h of HL^2 and it's complexes on MCF-7 cells.

24h	HL^2		$NiL^2{}_2$		$CuL^2{}_2$		$CoL^2{}_2$	
Doses(μM)	Viability (%)	Standard Deviation(±)	Viability (%)	Standard Deviation(±)	Viability (%)	Standard Deviation(±)	Viability (%)	Standard Deviation(±)
100	11.47	1.53	5.96	0.52	9.14	0.19	2.62	0.25
50	16.02	5.51	4.99	0.86	14.52	0.57	1.14	0.37
25	16.02	4.29	6.08	0.00	31.12	0.48	5.77	1.24
12.5	18.61	0.61	6.20	1.20	40.52	5.23	9.27	0.25
6.25	59.74	0.00	9.25	0.34	69.15	0.48	12.06	0.99
3.125	63.64	3.67	65.57	7.40	68.48	1.43	72.99	7.05
Control	100.00	14.08	100.00	25.12	100.07	0.86	100.00	16.57
IC_{50} (μM)	5.19		3.99		10.43		5.78	

Table 9
The viability percentages at 48 h of HL^1 and it's complexes on MCF-7 cells.

48h	HL^1		$NiL^1{}_2$		$CuL^1{}_2$		$CoL^1{}_2$	
Doses(μM)	Viability (%)	Standard Deviation(±)	Viability (%)	Standard Deviation(±)	Viability (%)	Standard Deviation(±)	Viability (%)	Standard Deviation(±)
100	0.00	30.30	10.89	2.27	8.20	1.50	3.15	0.00
50	27.98	4.21	15.89	1.77	10.98	9.17	2.85	0.00
25	47.32	2.95	25.18	0.76	8.60	6.55	9.35	0.14
12.5	56.25	4.63	42.14	2.02	12.30	7.67	8.66	1.53
6.25	77.68	0.42	46.25	5.30	16.93	1.50	17.91	0.28
3.125	90.48	10.10	41.96	1.77	24.87	7.86	30.81	4.18
Control	99.70	7.16	99.82	0.25	100.40	38.72	100.30	4.87
IC_{50} (μM)	21.25		7.78		2.17		2.35	

Table 10
The viability percentages at 48 h of HL^2 and it's complexes on MCF-7 cells.

48h	HL^2		$NiL^2{}_2$		$CuL^2{}_2$		$CoL^2{}_2$	
Doses(μM)	Viability (%)	Standard Deviation(±)	Viability (%)	Standard Deviation(±)	Viability (%)	Standard Deviation(±)	Viability (%)	Standard Deviation(±)
100	54.29	24.24	20.97	4.56	11.03	0.60	0.09	0.88
50	73.57	9.09	13.71	1.14	16.15	1.80	0.09	0.88
25	93.57	1.01	17.74	2.28	46.00	4.59	8.16	4.01
12.5	101.43	4.04	45.16	2.28	18.27	6.01	8.51	3.01
6.25	92.14	5.05	57.26	7.98	25.86	2.83	23.58	1.50
3.125	90.00	2.02	73.39	10.26	58.94	0.32	78.19	0.50
Control	85.71	10.10	100.00	4.56	99.62	1.62	102.22	5.14
IC_{50} (μM)	–		10.00		3.97		4.74	

These activity values were better than the values observed with 5-FU (5-fluorouracil, IC_{50}=4.7 μM), which is widely used in cancer treatment [53].

3.7. In-silico *ADMET results*

When identifying candidate molecules, it is critical to determine the pharmacokinetic properties of chemical compounds or drug candidate molecules, such as absorption, distribution, metabolism, and excretion (ADME). These parameters can help prevent these compounds from failing in clinical trials and increase their chances of becoming good drug candidates.

The ADME properties of the compounds were investigated for parameters such as molecular weight of the compounds (gr/mol),%Abs: Absorption percent, TPSA: Topological polar surface area, RB: number of rotatable bonds, HBA: number of hydrogen bond acceptors, HBD: number of hydrogen bond donors, LV: Number of 5 violations of the Lipinski rule, LogPo/w (iLOGP): Lipophilicity, BS: Bioavailability score, SA: synthetic accessibility and WS: water solubility. The data obtained are summarized in Table 11. While HL^1 and HL^2 obey the Lipinski rule, it is possible to say that the metal complexes do not obey only two rules. All compounds showed good compatibility regarding HBA, HBD and RB parameters and all of the compounds were expected to ve absorbed in the intesstines at high levels. Although the water solubility of the compounds ranged from low to very low. Since the TPSA values have to be less than the critical threshold 130, only HL^1 and HL^2 were found to conform this parameter. This case is violated since the molecular weight of the metal complexes is above 500. This is also the reason for the%abs. values. However, many of the commercially available molecules violate these rules, they are still used as drugs due to other prominent features.

Using the SwissADME online tool, the scale of similarity of synthetic compounds with the drug was used to estimate criteria such as lipophilicity, size, polarity, solubility, flexibility, and saturation. The ideal situation is that when these properties of the molecules are located in the pink region. That is to say when the basic constant properties are on the radar chart. The biocompatibility radar graphs of the compounds are given in Fig. 9. Except for saturation, the radar plot shows whether all the ligands, from which the complexes are synthesized, are in the pink area.

For some metal complexes data could not be obtained for some of the parameters since their molecular weights are above 500. However, as mentioned above, even for some widely used drug compound these parameters could not be compiled [54].

Moreover, the ADME properties of the compounds and their toxicity profiles were also investigated *in silico*. The pkCSM web tool [39]was used to obtain this information. Aside from the ADME properties of the compounds, their toxicity profiles were investigated *in silico*. The pkCSM web tool was used to obtain this information. This tool can predict lethal dose (LD_{50}), AMES Toxicity, hERG-I and hERG-II inhibitor, human maximum tolerated dose,

Table 11
Physicochemical and drug-likeliness properties of synthetic compounds according to RO5.

	MW	%Abs	TPSA(Å²)	RB	HBA	HBD	Log Po/w	LV	BS	SA	WS
	Rules										
Comp.	<500	>80	<130	≤ 9	≤ 10	≤ 5	≤ 5	≤ 1	–	–	–
HL^1	370.65	79.29	86.11	5	2	2	3.30	0	0.55	2.44	−5.61
$CoL^1{}_2$	801.25	57.22	150.08	6	6	3	4.75	2	0.17	6.06	−12.24
$CuL^1{}_2$	805.86	57.22	150.08	6	6	3	4.76	2	0.17	5.99	−12.24
$NiL^1{}_2$	801.01	57.22	150.08	6	6	3	4.75	2	0.55	6.02	−12.24
HL^2	326.17	74.76	99.25	5	3	2	2.23	0	0.55	2.55	−4.61
$CoL^2{}_2$	712.28	48.16	176.36	6	8	3	2.64	2	0.55	5.93	−9.93
$CuL^2{}_2$	716.89	48.16	176.36	6	8	3	2.64	2	0.55	5.86	−9.93
$NiL^2{}_2$	712.04	48.16	176.36	6	8	3	2.64	2	0.55	5.94	−9.93

Key: MW: Molecular weight (gr/mol). **%Abs**: Percentage of absorption. **TPSA:** Topological polar surface area. **RB:** number of rotatable bonds. **HBA:** number of hydrogen bond acceptors. **HBD:** number of hydrogen bond donors. **LV:** number of Lipinski rule of 5 violations. **Log Po/w** (iLOGP): Lipophilicity. **BS:** Bioavailability score. **SA:** Synthetic accessibility [From 1 (very easy) to 10 (very difficult)]. **WS:** Water solubility. Log *S* (Insoluable < −10 < Poorly < −6 < Moderately < −4 < Soluable < −2 Very < 0 < Highly).

LOAEL, Skin sensitization, T. pyriformis toxicity, Hepatotoxicity, and Minnow toxicity of compounds.

When the toxicity of the synthetic compounds are investigated, it is striking that none of the compounds were found to exhibit AMES toxicity. The hepatoxic effect of the HL^1 and the metal complexes derived from this ligand were observed to have negative effects while HL^2 and its metal complexes had positive effect. Moreover, not all compounds would cause skin sensitization.

The maximum tolerated dose, which should be ≥ 0.5 log (mg/kg/day), has values ranging from 0.071 log (mg/kg/day) to 0.495 log (mg/kg/day). Metal complexes of HL^2 had the lowest oral acute toxicity on rats, which was an LD_{50} value of 2.563 mol/kg. On the other hand, metal complexes of HL^1 had the lowest chronic oral toxicity on rats with 2.711 logs (mg/kg_bw/day). It was observed that all of the compounds showed T. *pyriformis* toxicity in the 0.285 to 1.092 log μg/L range, but since the lowest limit of Minnow toxicity is 0.5 mM only HL^1 and its metal complexes were found not to cause Minnow toxicity. Data regarding the predicted toxicity of compounds are given in Table 12.

3.8. Molecular docking study

Molecular docking analysis is one of the critical methods used in rational drug design, as it can examine the interaction between protein and ligands at the atomic level and predict the most stable structure and mode of interaction of the complex formed. This provided accurate information on identification and investigation of interaction in drug discovery and development [41,55]. Cancer develops due to the mutations built up in critical genes that disrupt the normal processes of cell proliferation, differentiation and death. B-type RAFkinase (BRAF), which is the most frequently mutated serine/threonine kinase in human cancers, is one of the main targets in drug research for cancer treatment [56,57]. Particularly, BRAF, which is a protein mutated at high frequency in melanoma, has become an ideal target for antitumor therapeutic development in many types of cancer [58] For this reason, BRAF (V600E) kinase was selected as the target protein, and molecular docking study was performed on the active site of BRAF for the synthesized molecules [59].

The intermolecular interactions between synthetic compounds and the receptor BRAF (4R5Y) were analyzed to reveal the binding modes of the best binding poses after molecular docking. 2D and 3D interactions were created to visualize and compare the binding modes of the compounds.When the binding affinities of the compounds are examined, the ligands HL^1 and the metal complexes -$CoL^1{}_2$ and $CuL^2{}_2$- have the highest scores. The values of binding affinities are higher than −8 kcal//mol for all compounds, and it is possible to say that the compounds form stable complexes via

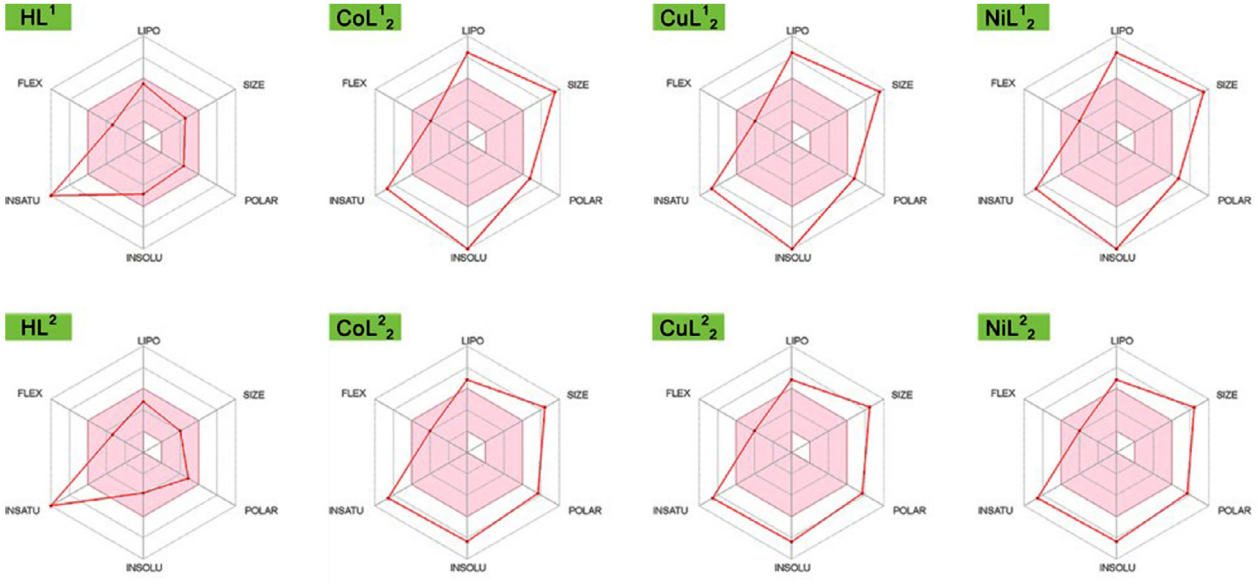

Fig. 9. Bioavailability radar related to the physicochemical properties of molecules.

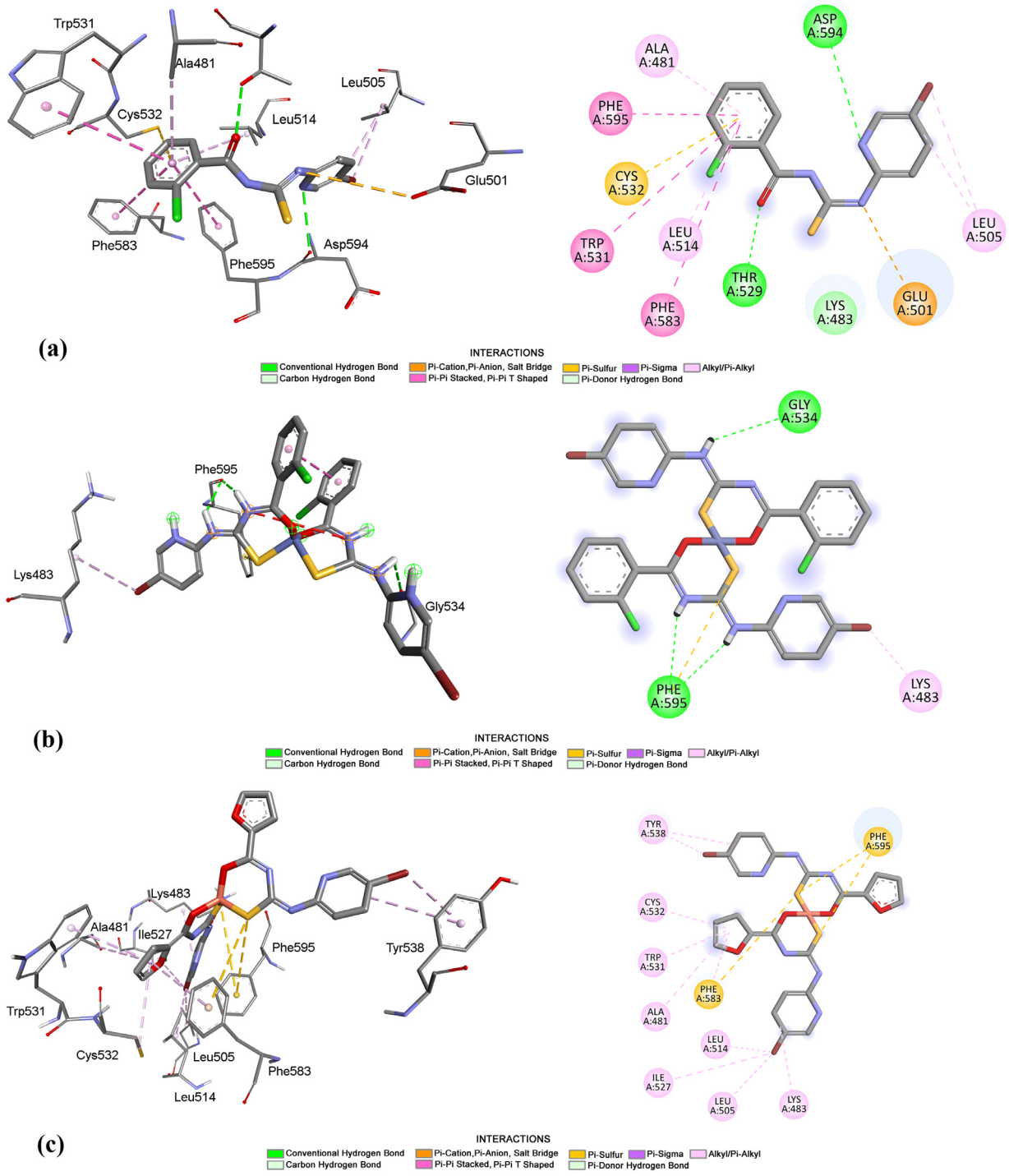

Fig. 10. 3D and 2D representations of the best pose interactions between the BRAF and compound HL^1 (a), $CoL^1{}_2$ (b), $CuL^2{}_2$ (c).

Table 12
Toxicity evaluation of compounds.

	Compounds							
Parameters	HL^1	$CoL^1{}_2$	$CuL^1{}_2$	$NiL^1{}_2$	HL^2	$CoL^2{}_2$	$CuL^2{}_2$	$NiL^2{}_2$
AMES toxicity	No	No	No	No	No	No	No	No
Max. Tolerated Dose	0.071	0.095	0.095	0.095	0.068	0.495	0.495	0.495
Oral Rat Acute Tox. (LD50)	2.760	2.711	2.711	2.711	2.571	2.563	2.563	2.563
Chronic Oral Rat Tox. (LOAEL)	1.138	1.110	1.110	1.110	0.504	0.002	0.002	0.002
Hepatotoxicity	No	No	No	No	Yes	Yes	Yes	Yes
Skin Sensitisation	No	No	No	No	No	No	No	No
T.Pyriformis toxicity	1.092	0.285	0.285	0.285	0.472	0.285	0.285	0.285
Minnow toxicity	−0.178	−1.081	−1.082	−1.079	2.383	1.057	1.055	1.058

Tabe 13
Interaction and amino acid residues are involved in the inhibition of BRAF summary.

Comp.	Binding affinity (kcal/mol)	Type of interaction bond	Involved receptor residues
HL^1	−8.3	HB, EC, HP, PS	GLU501, ASP594, TRP531, PHE583, PHE595, LEU505, ALA481, LEU514
$CoL^1{}_2$	−10.0	HB, HP, PS	PHE595, GLY534, LYS483
$CuL^1{}_2$	−9.3	HB, HP, PS	PHE595, GLU533, PHE583, HIS539, ILE463, LYS473, ALA481, TRP531
$NiL^1{}_2$	−9.9	HB, HP, PS	GLY534, GLU533, VAL471, PHE583, ALA543, ILE463, TRP531, TYR538
HL^2	−8.1	HB, HP, EC	ALA481, THR529, LYS483, GLU501, CYS532, ILE527, TRP531, PHE583
$CoL^2{}_2$	−9.0	HB, HP	GLY534, TRP531, VAL471, LEU514, ILE463, HIS539, PHE595
$CuL^2{}_2$	−9.9	HP, PS	PHE595, PHE583, LEU505, LEU514, LEU505, LYS483, ALA481, CYS532, TRP531, TYR538
$NiL^2{}_2$	−8.7	HB, EC, HP	GLU501, GLU594, ASP594, ILE573, LYS483, LEU514,

Key: HB: hydrogen bond.
C–HB: Carbon-Hydrogen Bond.
EC: electrostatic interaction.
HP: hydrophobic interaction.
PS: Pi-Sulfur.

strong interactions in the active site of the target protein. These values ranged from −8.1 to −10 kcal/mol for all compounds, with the highest binding affinity being −10.0 kcal/mol for compound $CoL^1{}_2$. The binding energies of the compounds, the residues with which they interact and the binding types formed are summarized in Table 13 and are given in detail in the supplementary file (Tables S15–S22).

When a general evaluation of the complexes was made, it was seen that synthetic compounds interact with residues such as PHE595, VAL471, CYS532, HIS539, PHE583, ALA481, THR529, LEU514, VAL482 and GLY464 that determine the active or inactive state of the BRAF protein. The binding modes for compounds bearing these amino acids confirm the importance of hydrophobic interaction. This can be explained by the predominance of hydrophobic binding types in the complexation interaction with the active site of BRAF. The protein-ligand interactions at specific binding sites of synthetic compounds are shown in Fig. 10(a)–(c).

4. Conclusion

N-((5-bromopyridin-2-yl)carbamothioyl)−2-chlorobenzamide (HL^1:$C_{13}H_9BrClN_3OS$), ***N***-((5-bromopyridin-2-yl)carbamothioyl) furan-2-carboxamide(HL^2:$C_{11}H_{10}BrN_3O_2S$) and their transition metal (Co (II). Ni (II) and Cu (II)) complexes were synthesized. They were characterized via elemental analysis, DTA-TG, FT-IR, UV–vis., ^{1}H NMR and magnetic susceptibility methods. The molecular structures of the ligands were elucidated via single-crystal X-ray diffraction. It was observed that while HL^1 crystallizes in the monoclinic system with the space group $P2_1/c$, and the number formula in the unit cell were found to be 4, HL^2 crystallizes in monoclinic system with the space group $P2_1/n$ and the number formula in the unit cell was found to be 4. The unit cell parameters for HL^1 were a = 6.694 Å, b = 13.846 Å, c = 15.763 Å. The unit cell parameters for HL^2 were a = 11.351 Å, b = 8.114 Å, c = 13.812 Å. The thermal behavior of the compounds was also examined. The synthesized ligands were observed to be thermally stable up to 119 °C and 134 °C, respectively. The results of the magnetic susceptibility studies showed that Cu(II) complexes had square planar geometry while the Co(II) and Ni(II) complexes had tetrahedral geometry. Cytotoxicity activities of the synthesized ligands and their complexes were determined via MTT assay against MCF-7 breast cancer cells. The IC_{50} values for MCF-7 cells were found to be in the range 2.07 µM – 21.7 µM. The results indicated that among all synthesized compounds, the $NiL^1{}_2$ complex was more cytotoxic when applied at a concentration of 2.07 µM for 24 h. The ADMET properties of the compounds were also extensively studied *in silico*. When the physicochemical, pharmacological and ADMET properties of HL^1 and HL^2 ligands were evaluated together with drug similarity parameters, it was found out that the compounds exhibited good drug-like behavior. Moreover, molecular docking studies were performed to evaluate the binding interactions between the compounds and BRAF (V600E -protein kinase). The results confirmed that all the synthesized compounds showed high binding affinity and had inhibitory effect against BRAF (V600E) protein kinase. When the results obtained with all *in vitro* and *in silico* approaches in this study are evaluated together, it can be concluded that the synthesized compounds are potent agents.

Declaration of Competing Interest

The authors declare no conflicts of interest.

CRediT authorship contribution statement

Tuncay Yeşilkaynak: Conceptualization, Methodology, Formal analysis, Investigation, Resources, Writing – original draft, Writing – review & editing, Visualization, Supervision, Project administration, Funding acquisition. **Fatma Nur Özkömeç:** Investigation, Visualization, Data curation. **Mustafa Çeşme:** Investigation, Visualization, Data curation. **Ruken Esra Demirdöğen:** Formal analysis, Resources, Writing – original draft, Writing – review & editing. **Emine Kutlu:** Investigation, Visualization, Data curation. **Hatice Mehtap Kutlu:** Methodology, Investigation, Resources, Writing – original draft. **Fatih Mehmet Emen:** Investigation, Visualization, Data curation.

Data Availability

Data will be made available on request.

Acknowledgments

The authors thanks Kahramanmaraş Sütçü İmam University Scientific Research Projects Unit (*Project codes: BAP-2019/3–13 M)* (Turkey) for funding. Crystallographic data for the structures reported in this paper have been deposited at the Cambridge Crystallographic Data centre (CCDC), CCDC 2125519 (HL^1) and CCDC 2125607 (HL^2).

Supplementary materials

Supplementary material associated with this article can be found, in the online version, at doi:10.1016/j.molstruc.2022.133758.

References

[1] E. Keskin, U. Solmaz, G. Binzet, I. Gumus, H. Arslan, Synthesis, characterization and crystal structure of platinum(II) complexes with thiourea derivative ligands, Eur. J. Chem. 9 (2018) 360–368, doi:10.5155/eurjchem.9.4.360-368.1774.

[2] J.R. Burgeson, A.L. Moore, J.K. Boutilier, N.R. Cerruti, D.N. Gharaibeh, C.E. Lovejoy, S.M. Amberg, D.E. Hruby, S.R. Tyavanagimatt, R.D. Allen, D. Dai, SAR analysis of a series of acylthiourea derivatives possessing broad-spectrum antiviral activity, Bioorg. Med. Chem. Lett. 22 (2012) 4263–4272, doi:10.1016/j.bmcl.2012.05.035.

[3] U. Solmaz, I. Gumus, G. Binzet, O. Celik, G.K. Balci, A. Dogen, H. Arslan, Synthesis, characterization, crystal structure, and antimicrobial studies of novel thiourea derivative ligands and their platinum complexes, J. Coord. Chem. 71 (2018) 200–218, doi:10.1080/00958972.2018.1427233.

[4] F. Karipcin, M. Atis, B. Sariboga, H. Celik, M. Tas, Structural, spectral, optical and antimicrobial properties of synthesized 1-benzoyl-3-furan-2-ylmethylthiourea, J. Mol. Struct. 1048 (2013) 69–77, doi:10.1016/j.molstruc.2013.05.042.

[5] H. Arslan, N. Duran, G. Borekci, C.K. Ozer, C. Akbay, Antimicrobial activity of some thiourea derivatives and their nickel and copper complexes, Molecules 14 (2009) 519–527, doi:10.3390/molecules14010519.

[6] D. Ugur, H. Arslan, N. Külcü, Synthesis, characterization and thermal behavior of 1,1-dialkyl-3-(4-(3,3- dialkylthioureidocarbonyl)-benzoyl)thiourea and its Cu(II), Ni(II), and Co(II) complexes, Russ. J. Coord. Chem./Koord. Khimiya 32 (2006) 669–675, doi:10.1134/S1070328406090089.

[7] T. Yesilkaynak, G. Binzet, F.M. Emen, U. Flörke, N. Külcü, H. Arslan, Theoretical and experimental studies on N-(6-methylpyridin-2-yl-carbamothioyl)biphenyl-4-carboxamide, Eur. J. Chem. 1 (2010) 1–5, doi:10.5155/eurjchem.1.1.1-5.3.

[8] Z. Weiqun, Y. Wen, Q. Lihua, Structure and stability of thiourea with water, DFT and MP2 calculations, J. Mol. Struct. THEOCHEM 730 (2005) 133–141, doi:10.1016/j.theochem.2005.06.012.

[9] G. Binzet, I. Gumus, A. Dogen, U. Flörke, N. Kulcu, H. Arslan, Nickel(II) and copper(II) complexes of N,N-dialkyl-N′-3-chlorobenzoylthiourea: synthesis, characterization, crystal structures, Hirshfeld surfaces and antimicrobial activity, J. Mol. Struct. 1161 (2018) 519–529, doi:10.1016/j.molstruc.2018.02.073.

[10] W. Yang, H. Liu, M. Li, F. Wang, W. Zhou, J. Fan, Synthesis, structures and antibacterial activities of benzoylthiourea derivatives and their complexes with cobalt, J. Inorg. Biochem. 116 (2012) 97–105, doi:10.1016/j.jinorgbio.2012.08.001.

[11] S. Saeed, N. Rashid, M. Ali, R. Hussain, Synthesis, characterization and antibacterial activity of nickel (II) and copper (II) complexes of N-(alkyl(aryl)carbamothioyl)-4-nitrobenzamide, Eur. J. Chem. 1 (2010) 200–205, doi:10.5155/eurjchem.1.3.200-205.120.

[12] R. del Campo, J.J. Criado, E. García, M.R. Hermosa, A. Jiménez-Sánchez, J.L. Manzano, E. Monte, E. Rodríguez-Fernández, F. Sanz, Thiourea derivatives and their nickel(II) and platinum(II) complexes: antifungal activity, J. Inorg. Biochem. 89 (2002) 74–82, doi:10.1016/S0162-0134(01)00408-1.

[13] E. Rodríguez-Fernández, J.L. Manzano, J.J. Benito, R. Hermosa, E. Monte, J.J. Criado, Thiourea, triazole and thiadiazine compounds and their metal complexes as antifungal agents, J. Inorg. Biochem. 99 (2005) 1558–1572, doi:10.1016/j.jinorgbio.2005.05.004.

[14] Z. Weiqun, Y. Wen, X. Liqun, C. Xianchen, N-Benzoyl-N′-dialkylthiourea derivatives and their Co(III) complexes: structure, and antifungal, J. Inorg. Biochem. 99 (2005) 1314–1319, doi:10.1016/j.jinorgbio.2005.03.004.

[15] C. Sacht, M.S. Datt, Synthesis and characterisation of mixed-ligand platinum(II)-sulfoxide complexes, [PtCl(DMSO)(L)], for potential use as chemotherapeutic agents (HL = N, N-dialkyl-N'-(3-R-benzoyl)thiourea), Polyhedron 19 (2000) 1347–1354, doi:10.1016/S0277-5387(00)00419-8.

[16] X.P. Rao, Y. Wu, Z.Q. Song, S. bin Shang, Z. de Wang, Synthesis and antitumor activities of unsymmetrically disubstituted acylthioureas fused with hydrophenanthrene structure, Med. Chem. Res. 20 (2011) 333–338, doi:10.1007/s00044-010-9303-8.

[17] H. Peng, Y. Liang, L. Chen, L. Fu, H. Wang, H. He, Efficient synthesis and biological evaluation of 1,3-benzenedicarbonyl dithioureas, Bioorg. Med. Chem. Lett. 21 (2011) 1102–1104, doi:10.1016/j.bmcl.2010.12.130.

[18] T. Yeşilkaynak, H. Muslu, C. Özpınar, F.M. Emen, R.E. Demirdöğen, N. Külcü, Novel thiourea derivative and its complexes: synthesis, characterization, DFT computations, thermal and electrochemical behavior, antioxidant and antitumor activities, J. Mol. Struct. 1142 (2017) 185–193, doi:10.1016/j.molstruc.2017.04.049.

[19] T. Yeşilkaynak, R.E. Demirdöğen, H. Muslu, F.M. Emen, Co(II), Ni(II), and Cu(II) metal complexes based on thiourea ligand: synthesis, characterization, thermal behaviors, anticancer, and antioxidant activities, Inorg. Nano-Met. Chem. (2021) 1–11, doi:10.1080/24701556.2021.1984532.

[20] V.K. Madan, A.D. Taneja, V.P. Kudesia, Synthesis and spectral studies of some pyrimidyl and thiazolyl substituted thioureas as potential fungicides and nematicides, J. Indian Chem. Soc. 68 (1991) 471–472.

[21] T. Yeşilkaynak, C. Özpınar, F.M. Emen, B. Ateş, K. Kaya, N -((5-chloropyridin-2-yl)carbamothioyl)furan-2-carboxamide and its Co(II), Ni(II) and Cu(II) complexes: synthesis, characterization, DFT computations, thermal decomposition, antioxidant and antitumor activity, J. Mol. Struct. 1129 (2017) 263–270, doi:10.1016/j.molstruc.2016.09.083.

[22] T. Yeşilkaynak, 2-Chloro-N-((5-chloropyridine-2-yl)carbamothioyl)benzamide and its Co(II), Ni(II) and Cu(II) metal complexes, J. Therm. Anal. Calorim. 124 (2016) 1029–1037, doi:10.1007/s10973-015-5221-9.

[23] H.M. Abosadiya, Synthesis, crystal structure and antioxidant evaluation of N-(4-formylpiperazine-1-carbonothioyl)benzamide, Eur. J. Chem. 11 (2020) 156–159, doi:10.5155/eurjchem.11.2.156-159.1981.

[24] K.J. Waldron, N.J. Robinson, How do bacterial cells ensure that metalloproteins get the correct metal? Nat. Rev. Microbiol. 7 (2009) 25–35, doi:10.1038/NRMICRO2057.

[25] K. Joyce, S. Saxena, A. Williams, C. Damurjian, N. Auricchio, S. Aluotto, H. Tynan, A.L. Demain, Antimicrobial spectrum of the antitumor agent, cisplatin, J. Antibiot. 63 (2010) 530–532, doi:10.1038/ja.2010.64.

[26] M.S. Peresin, Y. Habibi, J.O. Zoppe, J.J. Pawlak, O.J. Rojas, Nanofiber composites of polyvinyl alcohol and cellulose nanocrystals: manufacture and characterization, Biomacromolecules 11 (2010) 674–681, doi:10.1021/bm901254n.

[27] Synthesis and study of silver nanoparticles for antibacterial activity against Escherichia coli and Staphylococcus aureus, (2018). doi:10.1088/2043-6254/aac58f.

[28] J.S. Kim, E. Kuk, K.N. Yu, J.H. Kim, S.J. Park, H.J. Lee, S.H. Kim, Y.K. Park, Y.H. Park, C.Y. Hwang, Y.K. Kim, Y.S. Lee, D.H. Jeong, M.H. Cho, Antimicrobial effects of silver nanoparticles, nanomedicine: nanotechnology, Biol. Med. 3 (2007) 95–101, doi:10.1016/j.nano.2006.12.001.

[29] M. Arakha, S. Pal, D. Samantarrai, T.K. Panigrahi, B.C. Mallick, K. Pramanik, B. Mallick, S. Jha, Antimicrobial activity of iron oxide nanoparticle upon modulation of nanoparticle-bacteria interface OPEN, Sci. Rep. 5 (2015) 14813, doi:10.1038/srep14813.

[30] S. Halder, K.K. Yadav, R. Sarkar, S. Mukherjee, P. Saha, S. Haldar, S. Karmakar, T. Sen, Alteration of Zeta potential and membrane permeability in bacteria: a study with cationic agents, Springerplus (2015), doi:10.1186/s40064-015-1476-7.

[31] C.S. Alves, M.N. Melo, H.G. Franquelim, R. Ferre, M. Planas, L. Feliu, E. Bardají, W. Kowalczyk, D. Andreu, N.C. Santos, M.X. Fernandes, M.A.R.B. Castanho, Escherichia coli cell surface perturbation and disruption induced by antimicrobial peptides BP100 and pepR, J. Biol. Chem. 285 (2010) 27536–27544, doi:10.1074/jbc.M110.130955.

[32] G.M. Sheldrick, A short history of SHELX, Acta Crystallogr. Sect. A Found. Crystallogr. 64 (2008) 112–122, doi:10.1107/S0108767307043930.

[33] C.F. Macrae, I.J. Bruno, J.A. Chisholm, P.R. Edgington, P. McCabe, E. Pidcock, L. Rodriguez-Monge, R. Taylor, J. van de Streek, P.A. Wood, Mercury CSD 2.0 – new features for the visualization and investigation of crystal structures, J. Appl. Crystallogr. 41 (2008) 466–470, doi:10.1107/S0021889807067908.

[34] O.v. Dolomanov, L.J. Bourhis, R.J. Gildea, J.A.K. Howard, H. Puschmann, OLEX2 : a complete structure solution, refinement and analysis program, J. Appl. Crystallogr. 42 (2009) 339–341, doi:10.1107/S0021889808042726.

[35] H. Arslan, N. Külcü, U. Flörke, Synthesis and characterization of copper(II), nickel(II) and cobalt(II) complexes with novel thiourea derivatives, Trans. Met. Chem. 28 (2003) 816–819, doi:10.1023/A:1026064232260.

[36] T. Yeşilkaynak, 2-Chloro-N-((5-chloropyridine-2-yl)carbamothioyl)benzamide and its Co(II), Ni(II) and Cu(II) metal complexes: synthesis, characterization, thermal decomposition, electrochemical behavior and antioxidant activity, J. Therm. Anal. Calorim. 124 (2016) 1029–1037, doi:10.1007/s10973-015-5221-9.

[37] J. Han, T.P.N. Talorete, P. Yamada, H. Isoda, Anti-proliferative and apoptotic effects of oleuropein and hydroxytyrosol on human breast cancer MCF-7 cells, Cytotechnology 59 (2009) 45–53, doi:10.1007/s10616-009-9191-2.

[38] D.K. Isika, F.N. Özkömeç, M. Çeşme, O.A. Sadik, Synthesis, biological and computational studies of flavonoid acetamide derivatives, RSC Adv. 12 (2022) 10037–10050, doi:10.1039/D2RA01375D.

[39] D.E.V. Pires, T.L. Blundell, D.B. Ascher, pkCSM: predicting small-molecule pharmacokinetic and toxicity properties using graph-based signatures, J. Med. Chem. 58 (2015) 4066–4072, doi:10.1021/acs.jmedchem.5b00104.

[40] İ. Şahin, M. Çeşme, F.B. Özgeriş, Ö. Güngör, F. Tümer, Design and synthesis of 1,4-disubstituted 1,2,3-triazoles: biological evaluation, *in silico* molecular docking and ADME screening, J. Mol. Struct. 1247 (2022) 131344, doi:10.1016/j.molstruc.2021.131344.

[41] İ. Şahin, M. Çeşme, N. Yüce, F. Tümer, Discovery of new 1,4-disubstituted 1,2,3-triazoles: *in silico* ADME profiling, molecular docking and biological evaluation studies, J. Biomol. Struct. Dyn. (2022), doi:10.1080/07391102.2022.2025905.

[42] M.F. Emen, H. Arslan, N. Külcü, U. Flörke, N. Duran, Synthesis, characterization and antimicrobial activities of some metal complexes with N′-(2-chloro-benzoyl)thiourea ligands: the crystal structure of fac- [CoL3] and cis-[PdL2], Pol. J. Chem. 79 (2005) 1615–1626.

[43] A. Mohamadou, I. Déchamps-Olivier, J.P. Barbier, Copper, nickel and cobalt complexes with N,N-disubstituted′-benzoyl thioureas, Polyhedron 13 (1994) 1363–1370, doi:10.1016/S0277-5387(00)81702-7.

[44] T.S. Rao, K.L. Reddy, P. Lingaiah, Synthesis and structural studies of complexes of Co(II), Ni(II), Cu(II), Zn(II) and Cd(II) with substituted chalcones, Proc. Indian Acad. Sci. 100 (1988) 363–373, doi:10.1007/BF02840574.

[45] R. Selwin Joseyphus, M. Sivasankaran Nair, Synthesis, characterization and biological studies of some Co(II), Ni(II) and Cu(II) complexes derived from indole-3-carboxaldehyde and glycylglycine as Schiff base ligand, Arab. J. Chem. 3 (2010) 195–204, doi:10.1016/j.arabjc.2010.05.001.

[46] A.N.M.A. Alaghaz, R.A. Ammar, New dimeric cyclodiphosph(V)azane complexes of Cr(III), Co(II), Ni(II), Cu(II), and Zn(II): preparation, characterization and biological activity studies, Eur. J. Med. Chem. 45 (2010) 1314–1322, doi:10.1016/j.ejmech.2009.12.008.

[47] A.N.M.A. Alaghaz, H.A. Bayoumi, Y.A. Ammar, S.A. Aldhlmani, Synthesis, characterization, and antipathogenic studies of some transition metal complexes with N,O-chelating Schiff's base ligand incorporating azo and sulfonamide Moieties, J. Mol. Struct. 1035 (2013) 383–399, doi:10.1016/j.molstruc.2012.11.030.

[48] M. Sönmez, Synthesis and characterization of copper(II), nickel(II), cadmium(II), cobalt(II) and zinc(II) complexes with 2-Benzoyl-3-hydroxy-1-naphthylamino-3-phenyl-2-propen-1-on, Turk. J. Chem. 25 (2001) 181–185 https://journals.tubitak.gov.tr/chem/abstract.htm?id=4593.

[49] G. Binzet, F.M. Emen, U. Flörke, T. Yeilkaynak, N. Külcü, H. Arslan, 4-Chloro-N-[N-(6-methyl-2-pyridyl)carbamothioyl]benzamide, Acta Crystallogr. Sect. E Struct. Rep. Online 65 (2008), doi:10.1107/S1600536808041123.
[50] H. Arslan, U. Flörke, N. Külcü, M.F. Emen, Crystal structure and thermal behaviour of copper(II) and zinc(II) complexes with N-pyrrolidine-N′-(2-chlorobenzoyl)thiourea, J. Coord. Chem. (2006), doi:10.1080/00958970500270992.
[51] D. Onald EWEN, The sublimation of metals at low pressures, in: Proceedings of the Royal Society of London. Series A, Containing Papers of a Mathematical and Physical Character, 89, 1913, pp. 58–67, doi:10.1098/rspa.1913.0063.
[52] G. Binzet, H. Arslan, U. Flörke, N. Külcü, N. Duran, Synthesis, characterization and antimicrobial activities of transition metal complexes of N,N-dialkyl-N′-(2-chlorobenzoyl)thiourea derivatives, J. Coord. Chem. 59 (2006) 1395–1406, doi:10.1080/00958970500512633.
[53] W. Liu, J. Zhou, T. Zhang, H. Zhu, H. Qian, H. Zhang, W. Huang, R. Gust, Design and synthesis of thiourea derivatives containing a benzo[5,6]cyclohepta[1,2-*b*]pyridine moiety as potential antitumor and anti-inflammatory agents, Bioorg. Med. Chem. Lett. 22 (2012) 2701–2704, doi:10.1016/J.BMCL.2012.03.002.
[54] G. Kirishnamaline, J.D. Magdaline, T. Chithambarathanu, D. Aruldhas, A.R. Anuf, Theoretical investigation of structure, anticancer activity and molecular docking of thiourea derivatives, J. Mol. Struct. 1225 (2021) 129118, doi:10.1016/j.molstruc.2020.129118.
[55] D. Isika, M. Çeşme, F.J. Osonga, O.A. Sadik, Novel quercetin and apigenin-acetamide derivatives: design, synthesis, characterization, biological evaluation and molecular docking studies, RSC Adv. 10 (2020) 25046–25058, doi:10.1039/d0ra04559d.
[56] H.S.C. Tang, Y.C. Chen, Insight into molecular dynamics simulation of BRAF(V600E) and potent novel inhibitors for malignant melanoma, Int. J. Nanomed. 10 (2015) 3131–3146, doi:10.2147/IJN.S80150.
[57] J. Kim, B. Choi, D. Im, H. Jung, H. Moon, W. Aman, J.-.M. Hah, Computer-aided design and synthesis of 3-carbonyl-5-phenyl-1H-pyrazole as highly selective and potent BRAFV600E and CRAF inhibitor, J. Enzym. Inhib. Med. Chem. 34 (2019) 1314–1320, doi:10.1080/14756366.2019.1599366.
[58] H.B. El-Nassan, Recent progress in the identification of BRAF inhibitors as anticancer agents, Eur. J. Med. Chem. 72 (2014) 170–205, doi:10.1016/j.ejmech.2013.11.018.
[59] J.J. Liu, H. Zhang, J. Sun, Z.C. Wang, Y.S. Yang, D.D. Li, F. Zhang, H. bin Gong, H.L. Zhu, Synthesis, biological evaluation of novel 4,5-dihydro-2H-pyrazole 2-hydroxyphenyl derivatives as BRAF inhibitors, Bioorg. Med. Chem. 20 (2012) 6089–6096, doi:10.1016/J.BMC.2012.08.020.